Int. J. Anal. Appl. (2024), 22:203

International Journal of Analysis and Applications

Estimation of Epidemiological Parameters for COVID-19 Cases in Burkina Faso Using African Vulture Optimization Algorithm (AVOA)

Haoua Tinde[1], Adama Kiemtore[1], Wenddabo Olivier Sawadogo[1,2,*], Pengdewendé Ousséni Fabrice Ouedraogo[1,3], Ibrahim Zangré[3]

[1]*LANIBIO Laboratory University Joseph Ki-Zerbo, Ouagadougou, Burkina Faso*
[2]*LARED Laboratory University of Ouahigouya, Burkina Faso*
[3]*LaST Laboratory, University of Thomas SANKARA, Burkina Faso*

[*]*Corresponding author:* wenddabo81@gmail.com

Abstract. In this paper, we present a mathematical model that accounts for virus transmission through deceased individuals to simulate the dynamics of COVID-19 spread in Burkina Faso. The existence and uniqueness of the model's solution have been proven. The basic reproduction number was calculated using the Jacobian determinant method. The stability of the disease-free and endemic equilibrium points was studied. To estimate the model parameters, we used African Vulture Optimization Algorithm (AVOA). We then used this algorithm to estimate the parameters of the developed model using daily reported COVID-19 cases in Burkina Faso from March 11 to April 20, 2020. The results obtained show that the proposed model is more realistic for simulating the spread of COVID-19 in Burkina Faso.

1. Introduction

The coronavirus disease that emerged in December 2019 in the city of Wuhan, Hubei Province, China, highlighted the importance of mathematical modeling in the fight against infectious diseases. Several models have been created and tested in various countries [1–5]. Lamia et al. [6] developed two epidemiological models: one in 6D named SEIQRD (Susceptible-Exposed-Infected-Quarantined-Recovered-Deceased) to predict and estimate the state of the COVID-19 pandemic, and the other in 4D named SIRD (Susceptible-Infected-Recovered-Deceased) to analyze the long-term behavior of the pandemic. For this study, they used the nested sampling algorithm and the Extended Kalman Filter (EKF). H.B. Taboe and their collaborators [7] focused their study on forecasting the spread of COVID-19 in West Africa while considering control measures. Their approach is based on the analysis of the basic and controlled reproduction numbers. Yvette M. and

Received: Sep. 13, 2024.

2020 *Mathematics Subject Classification.* 35A01, 92B20, 34C11, 47H10.

Key words and phrases. COVID-19; mathematical model; parameters identification; AVOA algorithm.

https://doi.org/10.28924/2291-8639-22-2024-203
ISSN: 2291-8639

Robinah N. [8], proposed a mathematical model to evaluate the influence of vaccination programs on reducing the burden of COVID-19 in certain African countries through numerical sensitivity analysis. Aboudramane G. Et Al [9] developed a mathematical model to predict the spread of COVID-19 in Burkina Faso. Their study incorporated public policies to reduce the contact rate, allowing for better tracking of the evolution of these cases. But the parameters of the problem were not estimated based on real data.

Many studies in the literature have reported the risk of virus transmission through cadavers [10–13]. However, most of the models discussed do not account for this risk. This risk is not negligible in Burkina Faso, given that not all cases have been detected. In this work, we propose a variant of the SEIR model that incorporates virus transmission through corpses to simulate the spread of COVID-19 in Burkina Faso. But the parameters of the problem were not estimated based on real data.

The resulting mathematical model depends on several parameters that need to be identified. The function thus defined has a complex structure concerning the parameters and suffers from a lack of regularity. We propose using a metaheuristic method for solving it, as classical gradient-based methods do not yield good results.

Numerous metaheuristic algorithms have been presented in the literature to solve optimization problems [14–21]. In [23] Kiemtore et al. used the Grey Wolf Optimizer algorithm to estimate the parameters of a model describing the dynamics of hepatitis B in Burkina Faso.

In this work, we used African Vulture Optimization Algorithm (AVOA) a metaheuristic algorithm proposed by Benyamin Abdollahzadeh, Farhad Soleimanian Gharehchopogh, and Seyedali Mirjalili [44, 45].

The remainder of this paper is structured as follows: Section 2 is devoted to the presentation of the proposed mathematical model. Section 3 is devoted to the mathematical analysis of the model. The proof of global existence, uniqueness, and boundedness of solutions for the normalized system is presented. The basic reproduction number was calculated using the Jacobian method proposed by Baba Seidu et al. [38]. The stability of equilibrium points has also been studied. The parameter estimation problem has been formulated. In Section 4, we present the African Vulture Optimization Algorithm (AVOA) and its use for solving the parameter estimation problem. In Section 5, we present the results of the parameter estimation problem for the proposed model using reported COVID-19 case data from Burkina Faso from March 11 to April 20, 2020. A brief discussion of the obtained numerical results is provided. A sensitivity analysis was conducted to determine the most influential parameters of COVID-19 spread in Burkina Faso. The results show the ability of our model to simulate the real situation of COVID-19 in Burkina Faso. We conclude with Section 6.

2. Model Formulation

In this paper, we do formulation of the transmission dynamics of COVID-19. The model is given by five ordinary differential equations (ODEs) to illustrate the dynamic behavior of COVID-19 virus. The cumulative human population at any instant of time t represented by $N(t)$ is categorized in five different classes, namely $S(t)$ the susceptible individuals, $E(t)$ the exposed COVID-19 infected individuals, $I_d(t)$ the detected COVID-19 infected individuals, $I_u(t)$ the undetected COVID-19 infected individuals, $R(t)$ the individuals that have been recovered. Figure 1 represents the flow chart of the model which represents the flow compartments of all the variables taken from the population and Table 1 describes the parameters used in the model.

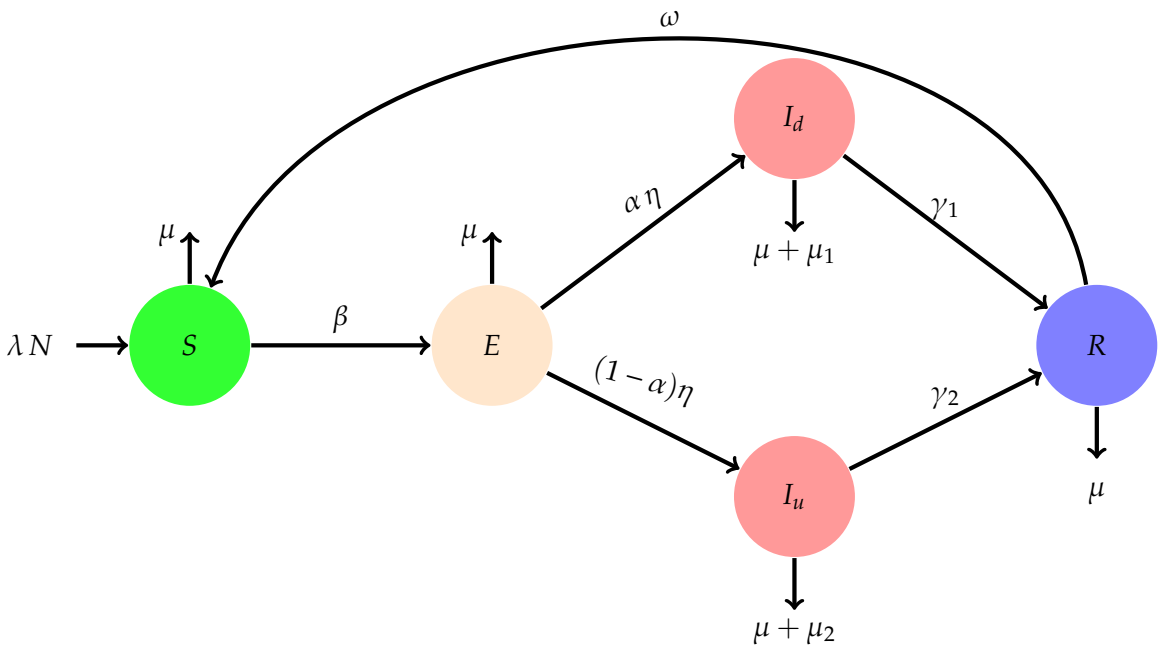

Figure 1. Diagram of the model of transmission of COVID-19

Parameter	description
λ	recruitment rate which comprises new births and immigrants
ω	losing immunity rate
σ	base-transmission rate
β_1	relative infectivity potential of detected infected
β_2	relative infectivity potential of undetected infected
τ	relative infectivity potential of dead undetected infected
α	proportion of cases that goes to the symptomatic class after the latency period
η	rate at which an exposed individual moves to the infectious class
μ	natural death rate of the human population
μ_1	mortality rate induced by COVID detected
μ_2	undetected COVID-induced mortality rate
γ_1	recovery rate of asymptomatic individuals
γ_2	recovery rate of symptomatic individuals

TABLE 1. Description of parameters used in the model

We now make the following assumptions:

(H_1) : The inflow of individuals into the population to enter the susceptible compartment is defined by λN (i.e recruitment rate which comprises new births and immigrants) [27].

(H_2) : In Burkina Faso, we divide infected individuals into two classes: detected or listed infected individuals and undetected infected individuals, i.e. those not listed by the health services.

(H_3) : In Burkina Faso, undetected dead infected individuals can transmit the virus during the burial process.

(H_4) : The force of new infection given by a standard incidence function and defines the following quantity:

$$\sigma\frac{\beta_1 I_d + (\beta_2 + \tau\,\mu_2)\, I_u}{N}$$

(H_5) : The appropriate contact coefficient for a susceptible person to become infected with COVID-19 depends on detected and undetected infected individuals ($\beta_1 I_d$ *and* $\beta_2 I_u$), as well as the deaths of undetected infected individuals $\tau\,\mu_2 I_u$.

(H_5) : All individuals who do not die from COVID-19, i.e. individuals in compartments S, E and R have the same natural mortality rate μ.

(H_6) : At any time $N(t) = S(t) + E(t) + I_d(t) + I_u(t) + R(t)$ represents the total size of the human population.

The susceptible population is generated by general recruitment λN and recovered individuals who become susceptible. This population is diminished by the newly infected individuals $\sigma\frac{\beta_1 I_d + (\beta_2 + \tau\,\mu_2)\, I_u}{N}$ and natural mortality μS. The following equation describes the dynamics of the susceptible :

$$\frac{dS}{dt} = \lambda N + \omega R - \sigma\frac{\beta_1 I_d + (\beta_2 + \tau\,\mu_2)\, I_u}{N} S - \mu S \tag{2.1}$$

The population of exposed compartment illustrates the susceptible individuals infection. This population is diminished by the transfer of this class μE and natural mortality μE. The dynamics of exposed individuals is given by the following equation:

$$\frac{dE}{dt} = \sigma \frac{\beta_1 I_d + (\beta_2 + \tau \mu_2) I_u}{N} S - (\eta + \mu) E \tag{2.2}$$

The exposed individuals move to the detected infected class with a rate $\alpha \eta$. The number of the population of the detected infected decreases by the mortalities (natural mortality μ and mortality induced by the disease μ_1) and also by the rate of recovered γ_1. For the infected individuals detected, we obtain the following equation:

$$\frac{dI_d}{dt} = \alpha \eta E - (\gamma_1 + \mu + \mu_1) I_d \tag{2.3}$$

Thus, the exposed individuals move again to the undetected infected class with a rate $(1-\alpha)\eta$. The number of the population of the undetected infected decreases by death rates (natural mortality μ and mortality induced by the disease μ_2) and also by the rate of recovered γ_2. For the infected individuals undetected, we obtain the following equation:

$$\frac{dI_u}{dt} = (1-\alpha) \eta E - (\gamma_2 + \mu + \mu_2) I_u \tag{2.4}$$

Finally, the recovered class, caracterized by the recuperation rates γ_1 and γ_2, is reduced by the natural mortality rate μ and the loss of immunity ω. The following differential equation expresses these dynamics:

$$\frac{dR}{dt} = \gamma_1 I_d + \gamma_2 I_u - (\mu + \omega) R \tag{2.5}$$

So combining all the differential equations formulated in (1)˘(5), we finally obtain the following system of COVID-19 dynamics equations:

$$\begin{cases} \dfrac{dS}{dt} = \lambda N + \omega R - \sigma \dfrac{\beta_1 I_d + (\beta_2 + \tau \mu_2) I_u}{N} S - \mu S \\ \dfrac{dE}{dt} = \sigma \dfrac{\beta_1 I_d + (\beta_2 + \tau \mu_2) I_u}{N} S - (\eta + \mu) E \\ \dfrac{dI_d}{dt} = \alpha \eta E - (\gamma_1 + \mu + \mu_1) I_d \\ \dfrac{dI_u}{dt} = (1-\alpha) \eta E - (\gamma_2 + \mu + \mu_2) I_u \\ \dfrac{dR}{dt} = \gamma_1 I_d + \gamma_2 I_u - (\mu + \omega) R \end{cases} \tag{2.6}$$

Posing

$$s = \frac{S}{N},\ e = \frac{E}{N},\ i_d = \frac{I_d}{N},\ i_u = \frac{I_u}{N},\ r = \frac{R}{N}$$

The normalized model of the model 2.6 is given by:

$$\begin{cases} \dfrac{ds}{dt} = \lambda + \omega\, r - \sigma\left(\beta_1 i_d + \beta_2 i_u + \tau\,\mu_2 i_u\right) s - \mu\, s \\ \dfrac{de}{dt} = \sigma\left(\beta_1 i_d + \beta_2 i_u + \tau\,\mu_2 i_u\right) s - (\eta + \mu)\, e \\ \dfrac{di_d}{dt} = \alpha\,\eta\, e - (\gamma_1 + \mu + \mu_1)\, i_d \\ \dfrac{di_u}{dt} = (1-\alpha)\,\eta\, e - (\gamma_2 + \mu + \mu_2)\, I_u \\ \dfrac{dr}{dt} = \gamma_1\, i_d + \gamma_2\, i_u - (\mu + \omega)\, r \\ s(0) = s_0,\ e(0) = e_0,\ i_d(0) = i_{d,0},\ i_u(0) = i_{u,0},\ r(0) = r_0 \end{cases} \tag{2.7}$$

3. Mathematical analysis of our Covid-19 model

3.1. **Properties of positivity and boundness.**

Theorem 3.1. *Consider the initial value*

$$(s_0,\ e_0,\ i_{d,0},\ i_{u,0},\ r_0) \in \mathbb{R}^5_+, \text{such that} \quad s_0 + e_0 + i_{d,0} + i_{u,0} + r_0 = 1$$

and

$$0 \le \lambda,\ \omega,\ \sigma,\ \beta_1,\ \beta_2,\ \tau,\ \theta,\ \mu,\ \mu_1,\ \mu_2,\ \eta,\ \alpha,\ \gamma_1,\ \gamma_2, \le 1$$

then there exists a unique, non negative, bounded global solution to system 3.1.
Moreover for all $t \ge 0$

$$\begin{aligned} &\Gamma = \left\{(s(t), e(t), i_d(t), i_u(t), r(t), d(t)) \in \mathbb{R}^5_+ |\ \ 0 \le Q(t) \le \frac{\lambda}{\mu} + Q_0\right\} \\ &0 \le s(t) \le \frac{\lambda}{\mu} \end{aligned} \tag{3.1}$$

where

$$Q(t) = s_(t) + e(t) + i_d(t) + i_u(t) + r(t) \ \ \textit{and} \ \ Q_0 = s_0 + e_0 + i_{d,0} + i_{u,0} + r_0 = 1 \tag{3.2}$$

Proof. To ensure local existence, all functions of system 3.1 must be locally Lipschitz continuous. As a result, a unique local solution exists on the interval $t \in [T_0, T_{max})$, where T_{max} represents the divergence time. The study of this type of system relies on basic techniques of ordinary differential equations. The assurance of unique solutions is obtained through various fixed point theorems on a maximal interval $[T_0, T_{max})$ [23,24]. By demonstrating that the components of the solution vector $(s(t),\ e(t),\ i_d(t),\ i_u(t),\ r(t)$ are uniformly bounded on any bounded interval $[0, T_{max})$, it is ensured

that $T_{max} = \infty$. We remark that the components of the vector

$$\mathcal{U}(s,e,i_d,i_u,r) = \begin{pmatrix} \mathcal{U}_1(s,\ e,\ i_d,\ i_u,\ r) \\ \mathcal{U}_2(s,\ e,\ i_d,\ i_u,\ r) \\ \mathcal{U}_3(s,\ e,\ i_d,\ i_u,\ r) \\ \mathcal{U}_4(s,\ e,\ i_d,\ i_u,\ r) \\ \mathcal{U}_5(s,\ e,\ i_d,\ i_u,\ r) \end{pmatrix} \tag{3.3}$$

Where

$$\begin{aligned} \mathcal{U}_1(s,\ e,\ i_d,\ i_u,\ r) &= \lambda + \omega\, r - \sigma\left(\beta_1 i_d + \beta_2 i_u + \tau\,\mu_2 i_u\right) s - \mu\, s \\ \mathcal{U}_2(s,\ e,\ i_d,\ i_u,\ r) &= \sigma\left(\beta_1 i_d + \beta_2 i_u + \tau\,\mu_2 i_u\right) s - (\eta + \mu)\, e \\ \mathcal{U}_3(s,\ e,\ i_d,\ i_u,\ r) &= \alpha\,\eta\, e - (\gamma_1 + \mu + \mu_1)\, i_d \\ \mathcal{U}_4(s,\ e,\ i_d,\ i_u,\ r) &= (1-\alpha)\,\eta\, e - (\gamma_2 + \mu + \mu_2)\, i_u \\ \mathcal{U}_5(s,\ e,\ i_d,\ i_u,\ r) &= \gamma_1\, i_d + \gamma_2\, i_u - (\mu + \omega)\, r \end{aligned} \tag{3.4}$$

are almost positive. Therefore, since the starting conditions are not negative, it follows that the solution components remain non-negative for each $t \in [T_0, T_{max})$. [22, 24]. Now, let the function Q be defined as :

$$Q(t) = s_(t) + e(t) + i_d(t) + i_u(t) + r(t) \tag{3.5}$$

By taking the sum of the first five equations in 3.1, one observes

$$\begin{cases} \dfrac{dQ}{dt} \leq \lambda - \mu Q(t) \\ Q(0) = s_0 + e_0 + i_{d,0} + i_{u,0} + r_0 = 1 \end{cases} \tag{3.6}$$

Integrating the equation 3.6 over $(0,t)$ for all $t_0 < t < T$, one can get the following

$$Q(t)e^{\mu t} - 1 \leq \frac{\lambda}{\mu}(e^{\mu t} - 1),$$

which implies that

$$Q(t) \leq e^{-\mu t} + \frac{\lambda}{\mu}(1 - e^{-\mu t}).$$

Therefore

$$Q(t) \leq (1 - \frac{\lambda}{\mu})e^{-\mu t} + \frac{\lambda}{\mu}.$$

Two distinct cases need to be examined here. If $\frac{\lambda}{\mu} < 1$, then the following inequality is satisfied

$$Q(t) \leq 1 - \frac{\lambda}{\mu} + \frac{\lambda}{\mu} \leq 1,$$

otherwise, if

$$\frac{\lambda}{\mu} \geq 1$$

then

$$Q(t) \leq \frac{\lambda}{\mu}.$$

In summary, we arrive at the following result, where $Q(t) \geq 0$

$$0 \leq Q(t) \leq \frac{\lambda}{\mu} + Q_0 \tag{3.7}$$

As a result, $T_{max} = \infty$ and it has been shown that a unique, non-negative, and bounded global solution exists.

We remark that $s(t)$ satisfies the following :

$$\begin{cases} \frac{ds}{dt} \leq \lambda - \mu\, s(t) \\ s(0) = s_0 \end{cases} \tag{3.8}$$

By integrating 3.7 over $[0, t]$ for all $t > 0$, one obtains:

$$\int_0^t \frac{d}{dp}\left(s(p)e^{\mu p}\right) \leq \int_0^t \lambda\, e^{\mu p} \tag{3.9}$$

This implies that

$$s(t)e^{\mu t} \leq \frac{\lambda}{\mu}\left(e^{\mu t} - 1\right) + s_0 \tag{3.10}$$

With

$$s_0 = \frac{\lambda}{\mu}$$

which implies that

$$0 \leq s(t) \leq \frac{\lambda}{\mu} \tag{3.11}$$

One can conclude the proof of this theorem. □

3.2. **Basic reproduction number and disease free-equilibrium $\mathcal{E}^0$.**

3.2.1. *Basic reproduction ratio.*

Theorem 3.2. *Consider the model 3.1 with the parameters specified in 3.1. Therefore,*

(i) *The equilibrium point in the absence of disease (DFE) is:*

$$\mathcal{E}^0 = \left(\frac{\lambda}{\mu},\ 0,\ 0,\ 0,\ 0\right) \tag{3.12}$$

(ii) *The basic reproduction number $\mathcal{R}_0$ of model is:*

$$\mathcal{R}_0 = \frac{\lambda\sigma\eta\left[\alpha\beta_1\left(\gamma_2+\mu+\mu_2\right)+\left(\gamma_1+\mu+\mu_1\right)\left(\beta_2+\tau\mu_2-\alpha\beta_2-\alpha\tau\mu_2\right)\right]}{\mu\left(\eta+\mu\right)\left(\gamma_1+\mu+\mu_1\right)\left(\gamma_2+\mu+\mu_2\right)} \tag{3.13}$$

Proof. Consider the model 3.1:

(i) To compute the equilibrium solutions, we set the right-hand-side of system to zero. One then obtains the disease-free equilibrium as follows :

$$\mathcal{E}^0 = \left(\frac{\lambda}{\mu},\ 0,\ 0,\ 0,\ 0\right) \tag{3.14}$$

(ii) The basic reproduction number $\mathcal{R}_0$, is calculated using the Jacobian-Determinant method of Baba Seidu described in the following ALgorithm [38]:

Step 1 :Identify the infected compartments of the model.
Step 2 : Find the Jacobian $\mathcal{J}$ of the infected subsystem of the model.
Step 3 : Evaluate the Jacobian of the infected subsystem at the disease-free equilibrium, $\mathcal{E}^0$ $\left(i.e\ \mathcal{J}\left(\mathcal{E}^0\right)\right)$.
Step 4 : Find the determinant, $\left|\mathcal{J}\left(\mathcal{E}^0\right)\right|$
Step 5 : Express the determinant as $\left|\mathcal{J}\left(\mathcal{E}^0\right)\right| = \xi\left(\frac{B}{D}-1\right)$
Step 6 : Find $\mathcal{R}_0$ using $\mathcal{R}_0 = \frac{B}{D}$

Thus let us consider only the infected compartments which satisfy the following third-order system :

$$\frac{d}{dt}\begin{pmatrix} e \\ i_d \\ i_u \end{pmatrix} = \begin{pmatrix} \sigma\left(\beta_1 i_d + \beta_2 i_u + \tau\,\mu_2 i_u\right)s - \left(\eta+\mu\right)e \\ \alpha\,\eta\,e - \left(\gamma_1+\mu+\mu_1\right)i_d \\ \left(1-\alpha\right)\eta\,e - \left(\gamma_2+\mu+\mu_2\right)i_u \end{pmatrix} \tag{3.15}$$

Adopting the notation $X = (e, i_d, i_u)$ for the infected states of model 3.1, one obtains the Jacobians:

$$\mathcal{J}(X) = \begin{pmatrix} -\left(\eta+\mu\right) & \sigma\beta_1 s_0 & \sigma(\beta_2+\mu_2\tau)s_0 \\ \alpha\,\eta & -\left(\gamma_1+\mu+\mu_1\right) & 0 \\ \left(1-\alpha\right)\eta & 0 & -\left(\gamma_2+\mu+\mu_2\right) \end{pmatrix} \tag{3.16}$$

$$\mathcal{J}\left(\mathcal{E}^0\right)=\begin{pmatrix} -(\eta+\mu) & \sigma\beta_1\dfrac{\lambda}{\mu} & \sigma(\beta_2+\tau\,\mu_2)\dfrac{\lambda}{\mu} \\ \alpha\,\eta & -(\gamma_1+\mu+\mu_1) & 0 \\ (1-\alpha)\,\eta & 0 & -(\gamma_2+\mu+\mu_2) \end{pmatrix} \tag{3.17}$$

Now,

$$\begin{aligned}\left|\mathcal{J}\left(\mathcal{E}^0\right)\right| &= (\eta+\mu)\,(\gamma_1+\mu+\mu_1)\,(\gamma_2+\mu+\mu_2) \\ &\left[\frac{\lambda\sigma\eta\,[\alpha\beta_1\,(\gamma_2+\mu+\mu_2)+(\gamma_1+\mu+\mu_1)\,(\beta_2+\tau\mu_2-\alpha\beta_2-\alpha\tau\mu_2)]}{\mu\,(\eta+\mu)\,(\gamma_1+\mu+\mu_1)\,(\gamma_2+\mu+\mu_2)}-1\right]\end{aligned} \tag{3.18}$$

Here we have,

$$\xi=(\eta+\mu)\,(\gamma_1+\mu+\mu_1)\,(\gamma_2+\mu+\mu_2)$$

□

Therefore,

$$\mathcal{R}_0=\frac{\lambda\sigma\eta\,[\alpha\beta_1\,(\gamma_2+\mu+\mu_2)+(\gamma_1+\mu+\mu_1)\,(\beta_2+\tau\mu_2-\alpha\beta_2-\alpha\tau\mu_2)]}{\mu\,(\eta+\mu)\,(\gamma_1+\mu+\mu_1)\,(\gamma_2+\mu+\mu_2)} \tag{3.19}$$

3.2.2. *Global stability of disease-free equilibrium point $\mathcal{E}^0$.*

This section presents the global stability analysis of the model at the disease-free equilibrium point. Next, we aim to provide a concise overview of the Castillo-Chavez method [26, 29, 30] to demonstrate the global stability of the system 2.7 at the disease-free equilibrium point. Thus, by applying the Castillo-Chavez method [26, 30], the given problem 2.7 is reformulated into the following sub-models:

$$\begin{cases}\dfrac{dX_1}{dt}=F(X_1,X_2), \\ \dfrac{dX_2}{dt}=G(X_1,X_2), \\ G(X_1,0)=0\end{cases} \tag{3.20}$$

Where X_1 and X_2 represent respectively the population of uninfected individuals and infected individuals.

The following conditions (C1) and (C2) must be satisfied to guarantee the local asymptotic stability.

(C1) If $\dfrac{dX_1}{dt}=F(X_1,0)$ then $\mathcal{E}^0$ is globally stable asymptotically.

(C2) $G(X_1,X_2)=BX_2-\hat{G}(X_1,X_2)$.

Where $\hat{G}(X_1,X_2)\geq 0$ for $(X_1,\ X_2)\in\Omega$, the matrix A is an M-matrix with quasi-positive off-diagonal elements. In the proposed model 3.1, $X_1=(s,r)\in\mathbf{R}^2$ and $X_1=(e,i_d,i_u)\in\mathbf{R}^3$. According to the

results obtained in *Section* 3.2.1 , The disease-free equilibrium point (DFE) is denoted by $\mathcal{E}^0$ and is defined as follows:

$$\mathcal{E}^0 = \left(\frac{\lambda}{\mu},\ 0,\ 0,\ 0,\ 0\right) \tag{3.21}$$

To ensure the global asymptotic stability of the disease-free equilibrium point, the results previously mentioned [26] were applied.

Theorem 3.3. *If $\mathcal{R}_0 < 1$ and $s(t) \leq \dfrac{\lambda}{\mu}$ then the DFE point $\mathcal{E}^0$ of the model 3.1 is globally asymptotically stable.*

Proof. In System 3.1, one can set the following

$$F(X_1, X_2) = \begin{pmatrix} \lambda + \omega\, r - \sigma\left(\beta_1 i_d + \beta_2 i_u + \tau\, \mu_2 i_u\right) s - \mu\, s \\ \\ \gamma_1\, i_d + \gamma_2\, i_u - (\mu + \omega)\, r \end{pmatrix} \tag{3.22}$$

and

$$G(X_1, X_2) = \begin{pmatrix} G_1(X_1, X_2) \\ \\ G_2(X_1, X_2) \\ \\ G_3(X_1, X_2) \end{pmatrix}$$

Where each part is described as follows:

$$G_1(X_1, X_2) = \sigma\left(\beta_1 i_d + \beta_2 i_u + \tau\, \mu_2 i_u\right) s - (\eta + \mu)\, e$$

$$G_2(X_1, X_2) = \alpha\, \eta\, e - (\gamma_1 + \mu + \mu_1)\, i_d$$

$$G_3(X_1, X_2) = (1 - \alpha)\, \eta\, e - (\gamma_2 + \mu + \mu_2)\, i_u$$

It is clear that $G(X_1, 0) = 0$ at the disease-free equilibrium point. We now need to demonstrate that (C_1) is satisfied.
To this aim, one calculates the eigenvalues of the Jacobian associate to $F(X_1, X_2)$ at $\mathcal{E}^0$.
Thus,

$$\mathcal{J}_F\left(\mathcal{E}^0\right) = \begin{pmatrix} -\mu & 0 \\ \\ 0 & 0 \end{pmatrix} \tag{3.23}$$

Since the only eigenvalue $\varsigma = -\mu$ found of the jacobian matrix is negative, then the DFE point $\mathcal{E}^0$ is globally asymptotically stable. To derive the condition (C_2), we first calculate the matrix

$B = \mathcal{J}_G(X_1, X_2)$ at the DFE point.

$$B = \begin{pmatrix} -(\eta+\mu) & \sigma\beta_1\dfrac{\lambda}{\mu} & \sigma\beta_2\dfrac{\lambda}{\mu} \\ \alpha\,\eta & -(\gamma_1+\mu) & 0 \\ (1-\alpha)\,\eta & 0 & -(\gamma_2+\delta+\mu) \end{pmatrix} \tag{3.24}$$

It is clear that the matrix B given above is an $M-$matrix with non-diagonal entries non-negative. Now, one can calculate the following fonction : $\hat{G}(X_1, X_2) = BX_2 - G(X_1, X_2)$ Then,

$$\bar{G}(X_1, X_2) = \begin{pmatrix} -(\eta+\mu) & \sigma\beta_1\dfrac{\lambda}{\mu} & \sigma(\beta_2+\tau\,\mu_2)\dfrac{\lambda}{\mu} \\ \alpha\,\eta & -(\gamma_1+\mu+\mu_1) & 0 \\ (1-\alpha)\,\eta & 0 & -(\gamma_2+\mu+\mu_2) \end{pmatrix} \times \begin{pmatrix} e \\ i_d \\ i_u \end{pmatrix} - \begin{pmatrix} \sigma\,(\beta_1 i_d + \beta_2 i_u + \tau\,\mu_2 i_u)\,s - (\eta+\mu)\,e \\ \alpha\,\eta\,e - (\gamma_1+\mu+\mu_1)\,i_d \\ (1-\alpha)\,\eta\,e - (\gamma_2+\mu+\mu_2)\,i_u \end{pmatrix} \tag{3.25}$$

$$\bar{G}(X_1, X_2) = \begin{pmatrix} \sigma\,\beta_1 i_d\left(\dfrac{\lambda}{\mu} - s\right) + \sigma(\beta_2+\tau\,\mu_2) i_u\left(\dfrac{\lambda}{\mu} - s\right) \\ 0 \\ 0 \end{pmatrix} \tag{3.26}$$

According to the theorem 3.1,

$$\sigma \geq 0,\ \beta_1 \geq 0,\ \beta_2 \geq 0,\ \lambda \geq 0,\ \mu \geq 0,\ \mu_1 \geq 0,\ \mu_2 \geq 0,\ \tau \geq 0$$

and

$$i_d(t) \geq 0,\ i_u(t) \geq 0,\ \frac{\lambda}{\mu} - s(t) \geq 0$$

Then,

$$\bar{G}(X_1, X_2) \geq 0$$

Consequently, the hypothesis (C_1) and (C_2) are satisfied. In addition, the Castillo-Chavez method ([26], [29], [37]) is used to establish that if $\mathcal{R}_0 < 1$, the disease-free equilibrium point exhibits global asymptotic stability. □

3.3. **Computation of the endemic steady-state $\mathcal{E}^*$.**

3.3.1. *Endemic equilibia $\mathcal{E}^*$.*

In presence of infected individuals, model 2.7 is said to be exhibiting an endemic equilibrium point
$\mathcal{E}^* = \left(s^*,\ e^*,\ i_d^*,\ i_u^*,\ r^*\right)$ where $s^*,\ e^*,\ i_d^*,\ i_u^*,\ r^*$ are given by :

$$\begin{aligned}
s^* &= \frac{\lambda\eta\left(\alpha\gamma_1(\gamma_2+\mu+\mu_2)+\gamma_2(1-\alpha)(\gamma_1+\mu+\mu_1)\right)}{\mu(\gamma_1+\mu+\mu_1)(\gamma_2+\mu+\mu_2)(\mu+\omega)\mathcal{R}_0};\\
e^* &= \frac{(\gamma_1+\mu+\mu_1)}{\alpha\eta}i_d^*;\\
i_u^* &= \frac{(1-\alpha)(\gamma_1+\mu+\mu_1)}{\alpha(\gamma_2+\mu+\mu_2)}i_d^*;\\
i_d^* &= \frac{\alpha\lambda\left(\eta\alpha\gamma_1(\gamma_2+\mu+\mu_2)+\eta\gamma_2(1-\alpha)(\gamma_1+\mu+\mu_1)-(\gamma_1+\mu+\mu_1)(\gamma_2+\mu+\mu_2)(\mu+\omega)\mathcal{R}_0\right)}{(\gamma_1+\mu+\mu_1)\mathcal{R}_0\left(\alpha\gamma_1(\gamma_1+\mu+\mu_1)+\gamma_2(1-\alpha)(\gamma_1+\mu+\mu_1)\right)(\omega-(\eta+\mu))};\\
r^* &= \frac{\alpha\gamma_1(\gamma_2+\mu+\mu_2)+\gamma_2(1-\alpha)(\gamma_1+\mu+\mu_1)}{\alpha(\gamma_2+\mu+\mu_2)(\mu+\omega)}i_d^*;
\end{aligned} \tag{3.27}$$

3.3.2. *Global stability of endemic equilibrium point $\mathcal{E}^*$.*

In this section, by using a suitable Lyapunov function, we will show that the endemic equilibrium point is globally asymptotically stable $\mathcal{E}^*$.

Theorem 3.4. *If $\mathcal{R}_0 > 1$, the endemic equilibrium point $\mathcal{E}^*$ of system 2.7 is globally asymptotically stable.*

Proof. When $\mathcal{R}_0 > 1$, one defines the following Lyapunov function as in [27,28,31,32,35]:

$$\mathcal{L} = (s-s^*)+(e-e^*)+\left(i_d-i_d^*\right)+(i_u-i_u^*)+(r-r^*)-\left(s^*+e^*+i_d^*+i_u^*+r^*\right)\times ln\left(\frac{s+e+i_d+i_u+r}{s^*+e^*+i_d^*+i_u^*+r^*}\right) \tag{3.28}$$

As $Q = s+e+i_d+i_u+r$, one can set $Q^* = s^*+e^*+i_d^*+i_u^*+r^*$ Subsequently, the Lyapunov function can also be reformulated as follows

$$\begin{aligned}
\mathcal{L} &= Q-Q^*-Q^*ln\frac{Q}{Q^*}\\
\mathcal{L} &= Q^*\left(\frac{Q}{Q^*}-1-ln\frac{Q}{Q^*}\right)
\end{aligned} \tag{3.29}$$

We will use the family of Volterra-type Lyapunov functions given by $g(x) = x-1-\ln(x)$, $x \in \mathbf{R}^+$, which has a global minimum at $x = 1$ and satisfies $g(1) = 0$.
Since $s(t) > 0,\ e(t) > 0,\ i_d(t) > 0,\ i_u(t) > 0,\ r(t) > 0,$, then one can obtain the following

$$\mathcal{L} = Q-Q^*-Q^*ln\frac{Q}{Q^*} > 0 \tag{3.30}$$

Therefore, the Lyapunov function $\mathcal{L}$ derivative is given by the following sense

$$\frac{d\mathcal{L}}{dt} = \left(1-\frac{Q^*}{Q}\right)\frac{dQ}{dt} \tag{3.31}$$

Note that according to system 2.7

$$\frac{dQ}{dt} = \lambda - \mu_1 i_d - \mu_2 i_u - \mu Q \tag{3.32}$$

As at the endemic equilibrium point $\frac{dQ}{dt} = 0$, then one obtains

$$\lambda = \mu_1 i_d + \mu_2 i_u + \mu Q \tag{3.33}$$

From 3.3.2, 3.3.2, and by assuming that

$$Q - Q^* \geq 0,\ i_d - i_d^* \geq 0,\ i_u - i_u^* \geq 0 \tag{3.34}$$

One has

$$\begin{aligned}
\frac{d\mathcal{L}}{dt} &= \left(1 - \frac{Q^*}{Q}\right)\left(\mu_1 i_d + \mu_2 i_u + \mu Q - \mu_1 i_d^* - \mu_2 i_u^* \mu Q^* - \mu Q\right) \\
\frac{d\mathcal{L}}{dt} &= -\left(\frac{Q - Q^*}{Q}\right)\left[\mu_1\left(i_d - i_d^*\right) + \mu_2\left(i_u - i_u^*\right) + \mu\left(Q - Q^*\right)\right] \\
\frac{d\mathcal{L}}{dt} &\leq 0
\end{aligned} \tag{3.35}$$

From (3.2) and by using the fact that $\frac{d\mathcal{L}}{dt} = 0$ if and only if
$s = s^*,\ e = e^*,\ i_d = i_d^*,\ i_u = i_u^*, r = r^*$, then $\frac{d\mathcal{L}}{dt}$ converges in positive region Φ such as t $\longrightarrow \infty$.
In accordance with LaSalle's invariance principle theorem [35],the endemic equilibrium point $\mathcal{E}^*$ is characterized by global asymptotic stability when $\mathcal{R}_0 > 1$ [32, 36]. □

3.4. **Parameters estimation.**

Let thus M observations of values of detected infected $I_{obs}(t_j)$ at the moments t_j, $j = 1, \ldots, M$.
At the problem 2.6, We assign the following definition to the functional J

$$J(U) = \int_{t_i}^{t_f} (I_d(t) - I_{obs}(t))^2 dt \tag{3.36}$$

$U = (\beta_1, \beta_2, \sigma, \eta, \alpha, \gamma_1, \gamma_2, \mu_1, \mu_2, \tau)$ is the vector of parameters to determinate.
t_i the initial time and t_f the final time.
The parameters estimation problem consists in solving

$$\min_{U \subset \mathcal{D}} J(U) \tag{3.37}$$

where $\mathcal{D} = [0, 1]^{10}$ a bounded subset of $\mathbb{R}^{10}$.
The problem defined by 3.36 has a unique solution.

4. Presentation of African Vulture Optimization Algorithm (AVOA)

African Vulture Optimization Algorithm (AVOA) is a metaheuristic algorithm proposed by Benyamin Abdollahzadeh Et al. [44, 45]. This algorithm was developed based on the modeling and simulation of the life habits and foraging behavior of African vultures. The assumptions of AVOA are as follows:

- The population consists of N vultures. This population can be divided into three groups based on the vultures' life habits.
- The position space of each vulture is indicated in d dimensions. It is determined by the fitness value of the feasible solution. The first best vulture corresponds to the best solution, the second vulture to the second-best solution, and the remaining vultures to the third group of the population.
- The separation of the three groups is created to formulate the most crucial natural function of vultures, which is living in groups to find food. Therefore, each group differs in its ability to find and obtain food.
- The vultures' habits and behavior, which involve searching for food for hours, allow them to avoid the traps of hunger. The strongest and most efficient vultures correspond to the best vultures, while the weakest and hungriest vultures correspond to the worst vultures. In AVOA, vultures seek to approach the best vultures while avoiding the worst ones.

4.1. **The Steps of AVOA.**

The AVOA algorithm consists of four stages. [44, 45]

⋆ Phase 1: Population Grouping

Once the initial population is generated, the fitness values of all solutions are calculated. The best solution represents the best vulture of the first group, while the second-best solution represents the best vulture of the second group. Based on equation (4.1), the other solutions are oriented towards the best solutions of the first and second groups.

$$R(i) = \begin{cases} BestVulture_1 & \text{if } p_i = L_1 \\ BestVulture_2 & \text{if } p_i = L_2 \end{cases} \quad \text{où } i = 1, \ldots, N. \tag{4.1}$$

where $R(i)$: selected best vulture

BestVulture$_1$: the best vulture of the first group

BestVulture$_2$: the best vulture of the second group

L_1 and L_2: parameters to be measured before the operation, ranging from [0,1]

The probability of selecting the best solution from each group, p_i, is determined according to the roulette wheel mechanism by equation (4.2):

$$p_i = \frac{F_i}{\sum_{i=1}^{n} F_i} \tag{4.2}$$

where F_i is the fitness of the vulture i and n is the total number of vultures in the two groups.

★ Phase 2: The Rate of Starvation of Vultures F

When vultures are well-fed, they have high energy to search for food over long distances. On the other hand, when they are hungry, they become aggressive and lack the energy to fly long distances, staying close to the stronger vultures that have food. Equation (4.3) allows the transition from the exploration phase to the exploitation phase, inspired by the vultures' satiety or hunger rate. The modeling of this behavior is given by equation (4.3). [44, 45]

$$F = (2 \times rand_1 + 1) \times z \times \left(1 - \frac{\text{iteration}_i}{\text{maxiterations}}\right) + t \tag{4.3}$$

where:

$rand_1$: a random value between 0 and 1

z: a random value in the interval [-1, 1] that changes at each iteration

with:

$$t = h \times \left(\sin\left(\omega \times \frac{\pi}{2} \times \frac{\text{iteration}_i}{\text{maxiterations}}\right) + \cos\left(\frac{\pi}{2} \times \frac{\text{iteration}_i}{\text{maxiterations}}\right) - 1\right) \tag{4.4}$$

where:

h: a random number between [-2, 2]

w: a constant controlling the exploration phase

When the value $|F_i|$ is greater than 1, the vultures enter the exploration phase and search for food in different locations. Otherwise, they enter the exploitation phase, seeking food nearby.

★ Phase 3: Exploration Phase

At this stage, the AVOA is examined. In nature, vultures have very good visual capabilities, allowing them to efficiently find food and detect dying animals. In AVOA, vultures use two strategies to explore randomly selected locations. Each strategy is chosen using a parameter P_1 ranging from 0 to 1. The model is:

$$P(i+1) = \begin{cases} \text{equation (4.6) si } P_1 \geq \text{randP}_1 \\ \text{equation (4.8) si } P_1 < \text{randP}_1 \end{cases} \tag{4.5}$$

$$P(i+1) = R(i) - D(i) \times F \tag{4.6}$$

$$D(i) = |X \times R(i) - P(i)| \tag{4.7}$$

where:

$R(i)$: one of the chosen best vultures

$P(i)$: current position vector of the vulture

$P(i+1)$: position vector of the vulture at the next iteration

$$P(i+1) = R(i) - F + \text{rand2} \times ((ub - lb) \times \text{rand3} + lb) \tag{4.8}$$

with:
$rand_2$: a random number between [0, 1]
$D(i)$: distance between the vulture and the current optimum
$rand_3$: used to provide a high random coefficient
lb and ub: lower and upper bounds
X: a random value between 0 and 2

⋆ Phase 4: Exploitation Phase (First Step)
The first step of the exploitation phase begins when the value of $|F_i|$ is between [0.5, 1]. In this phase, two behaviors are performed: rotational flight and siege fighting. The parameter P_2, ranging from [0, 1], is chosen to allow the selection of each strategy, which must be chosen before each search operation. At the start of each phase, a random number $rand_{p2}$ between 0 and 1 is generated. If this number is less than P_2, the rotational flight strategy is implemented. If this number is greater than or equal to P_2, the siege fighting is applied slowly. This step is simulated as follows: [44,45]

$$P(i+1) = \begin{cases} \text{Eq.(4.10)} & \text{si } P_2 \geq \text{randp}_2, \\ \text{Eq.(4.12)} & \text{si } P_2 < \text{randp}_2, \end{cases} \quad i = 1, \ldots, N. \tag{4.9}$$

$$P(i+1) = D(i) \times (F + \text{rand}_4) - d(t), \quad i = 1, \ldots, N. \tag{4.10}$$

$$P(i+1) = R(i) - (S_1(i) + S_2(i)), \quad i = 1, \ldots, N. \tag{4.11}$$

where:
$rand_4$: a random number in [0, 1]
$d(i)$: distance between the i-th vulture and the current best vulture, calculated as follows:

$$d(i) = R(i) - P(i), \quad i = 1, \ldots, N. \tag{4.12}$$

$S_1(i)$ and $S_2(i)$ are calculated in (4.13) and (4.14):

$$S_1(i) = R(i) \times \left(\frac{\text{rand}_5 \times P(i)}{2\pi} \right) \times \cos(P(i)), \quad i = 1, \ldots, N. \tag{4.13}$$

$$S_2(i) = R(i) \times \left(\frac{\text{rand}_6 \times P(i)}{2\pi} \right) \times \sin(P(i)), \quad i = 1, \ldots, N. \tag{4.14}$$

with: rand_5 and rand_6 are random numbers between 0 and 1.

⋆ Phase 5: Exploitation Phase (Second Step)
This phase is initiated if $|F_i| < 0.5$. The movements of the two best vultures gather several types of vultures around the same food source, but siege and aggressive fighting to find food are performed. Before the vultures act, a random number $rand_{P3}$ between 0 and 1 is generated. There is a parameter $P3$ such that if $rand_{P3}$ is greater than or equal to $P3$, multiple types of vultures gather

around the same food source. If $rand_{P3}$ is less than $P3$, the aggressive fighting and siege strategy is implemented. This phase is simulated as follows:

$$P(i+1) = \begin{cases} \text{Eq.(4.16)} & \text{if } P_3 \geq \text{rand}_{p3} \\ \text{Eq.(4.17)} & \text{if } P_3 < \text{rand}_{p3} \end{cases}, \quad i = 1, \ldots, N. \tag{4.15}$$

$$P(i+1) = \frac{A_1(i) + A_2(i)}{2}, \quad i = 1, \ldots, N. \tag{4.16}$$

$$P(i+1) = R(i) - d(i) \times F \times \text{Levy}(d), \quad i = 1, \ldots, N. \tag{4.17}$$

where: d is the dimension of the problem
A_1 and A_2 are calculated by (4.18)and (4.19), respectively

$$A_1(i) = \frac{\text{Best Vulture}_1(i)}{\text{Best Vulture}_1(i) - (P(i))^2} \times P(i) \times F, \quad i = 1, \ldots, N. \tag{4.18}$$

$$A_2(i) = \frac{\text{Best Vulture}_2(i)}{\text{Best Vulture}_2(i) - (P(i))^2} \times P(i) \times F, \quad i = 1, \ldots, N. \tag{4.19}$$

The Lévy flight mechanism increases the efficiency of AVOA. Its formula is:

$$Levy(d) = 0.01 \times \frac{r_1 \times \sigma}{r_2^{\frac{1}{\beta}}} \tag{4.20}$$

where β is a fixed number equal to 1.5; r_1 and r_2 are random numbers between 0 and 1. σ can be calculated as shown in equation (4.21)

$$\sigma = \left(\frac{\Gamma(1+\beta) \times \sin\left(\frac{\pi\beta}{2}\right)}{\Gamma\left(\frac{1+\beta}{2}\right) \times \beta \times 2 \times \left(\frac{\beta-1}{2}\right)} \right)^{\frac{1}{\beta}} \tag{4.21}$$

où $\Gamma(x) = (x-1)!$

4.2. **The pseudo-code of the AVOA.**

The pseudo-code of the AVOA is described in following algorithm: [44, 45].

Algorithm AVOA for parameter estimation problem

Inputs: Population dimension N and maximum number of iterations T
Outputs: The location of Vulture and its fitness value
Initialize the random population $P_i(i = 1, 2, \ldots, N)$
while (stopping condition is not met) **do**
Solve the direct problem 2.6
Calculate the fitness values of Vulture using cost function 3.36
Set $P_{\text{BestVulture}_1}$ to represent the Vulture's position (Best position for Vulture Category 1)
Set $P_{\text{BestVulture}_2}$ to represent the Vulture's position (Second best location Best Vulture Category 2)
for (each Vulture (P_i)) **do**
Select $R(i)$ Eq.(4.1)
Update the F) Eq. (4.3)
if $(|F| \geq 1)$ **then**
if $(P_1 < \text{rand}_{P_1})$ **then**
Update the location Vulture Eq. (4.6)
else
Update the location Vulture Eq. (4.8)
end if
else if $(|F| < 1))$ **then**
if $(|F| \geq 0.5)$ **then**
if $(P_2 < \text{rand}_{P_2})$ **then**
Update the location Vulture Eq. (4.10)
else
Update the location Vulture Eq. (4.11)
end if
else
if $(P_3 \geq \text{rand}_{P_3})$ **then**
Update the location Vulture Eq. (4.16)
else
Update the location Vulture Eq. (4.17)
end if
end if
end if
end for
end while
return $P_{\text{BestVulture}_1}$

5. Results and Discussion

5.1. **Findings from parameter estimation.**

The statistics we used are the daily COVID-19 cases reported in Burkina Faso from March 11 to April 20, 2020.

The initial values used are $S(0) = 20840800, E(0) = 131, I_d(0) = 2, I_u(0) = 4, R(0) = 0$

. You will find the parameter values used in the table below.

Parameters	description	Values	references
λ	recruitment rate	$0.00075/day$	Assumed
μ	natural mortality rate	0.0165	[34]
ω	losing immunity rate	0.55	Assumed

The table presents the results of the parameter estimation problem using AVOA algorithm

Parameters	ranges	estimated values
β_1	$[0.4 - 0.8]$	0.5
β_2	$[0.4 - 0.9]$	0.8
σ	$[0.4 - 0.8]$	0.75
η	$[0.1 - 0.3]$	0.3
α	$[0.2 - 0.4]$	0.4
γ_1	$[0.1 - 0.3]$	0.15
γ_2	$[0.1 - 0.2]$	0.2
μ_1	$[0 - 0.02]$	0.008
μ_2	$[0 - 0.02]$	0.01
τ	$[0 - 0.02]$	0.0149

Table 2. Estimated parameters

The figure (2) presents both the observed data and the estimated data.

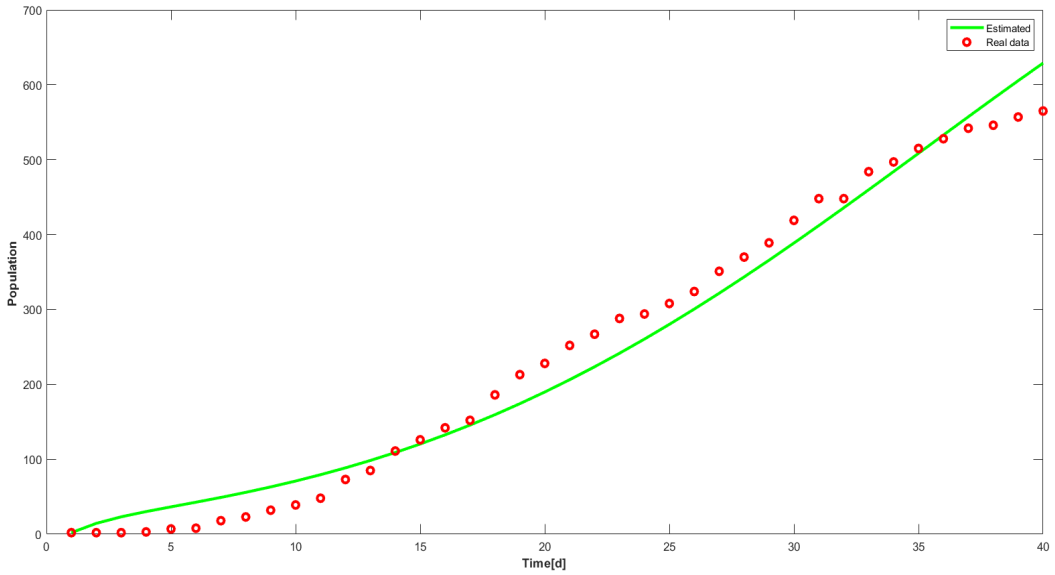

FIGURE 2. The daily covid-19 cases time series in Burkina Faso from March 11 to April 20, 2020 and the best-fitting curve of the proposed model

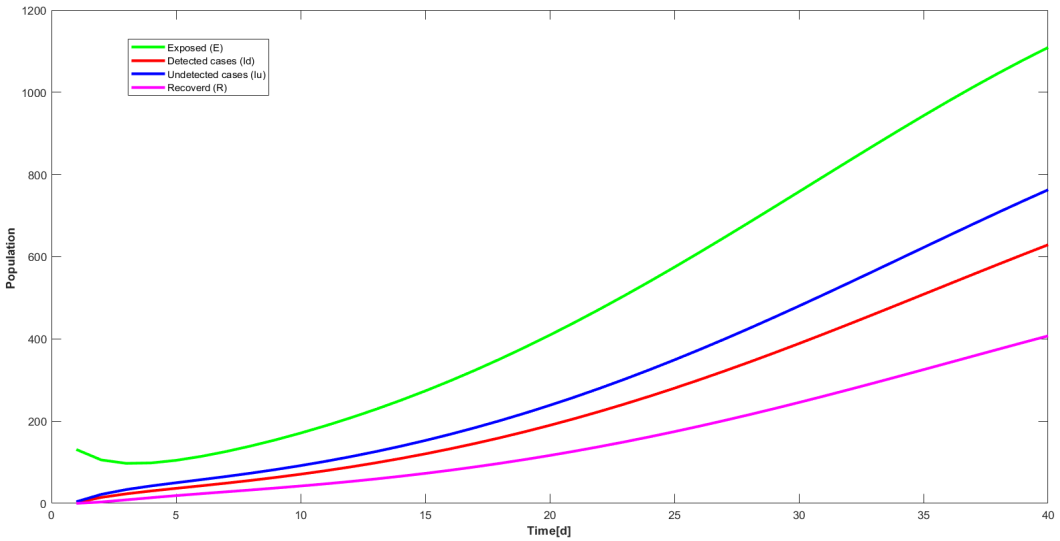

FIGURE 3. Evolution of population

After the numerical simulation with the estimated parameters, the figure (3) shows the evolution of the number of exposed infected individuals, detected infected individuals, undetected infected individuals, and recovered individuals in the population of Burkina Faso. Additionally, the obtained value for the basic reproduction number is $R_0 = 1.0597 > 1$.

5.2. **Sensitivity analysis.**

Sensitivity analysis is a method used to determine how fluctuations in model parameters influence the results. The effect of each parameter on the endemic threshold has been described in the sensitivity analysis for Covid-19 virus transmission. The parameter with the lowest sensitivity index magnitude is less significant than the one with the highest sensitivity index magnitude. Sensitivity indices of parameters can be either positive or negative. The sensitivity analysis that we will perform will help us understand how variations in parameters influence our dynamic model (2.7). The sensitivity index of the parameter Υ for $\mathcal{R}_0$ is calculated using the following formula: [46, 47]:

$$\chi_{\Upsilon}^{\mathcal{R}_0} = \frac{\partial \mathcal{R}_0}{\partial \Upsilon} \times \frac{\partial \Upsilon}{\mathcal{R}_0} \approx \frac{\%\Delta R_0}{\%\Delta p} \tag{5.1}$$

From equation(3.13), we obtain:

$$\chi_{\mu_1}^{R_0} = -\frac{\lambda\sigma\eta\alpha\beta_1}{\mu(\eta+\mu)(\gamma_1+\mu+\mu_1)^2} \tag{5.2}$$

$$\chi_{\mu_2}^{R_0} = \frac{\lambda\sigma\eta\left[(\tau-\alpha\tau)(\gamma_2+\mu+\mu_2)-(\beta_2+\tau\mu_2-\alpha\beta_2-\alpha\tau\mu_2)\right]}{\mu(\eta+\mu)(\gamma_2+\mu+\mu_2)^2} \tag{5.3}$$

$$\chi_{\beta_1}^{R_0} = \frac{\lambda\sigma\eta\alpha(\gamma_2+\mu+\mu_2)}{\mu(\eta+\mu)(\gamma_1+\mu+\mu_1)(\gamma_2+\mu+\mu_2)} \tag{5.4}$$

$$\chi_{\beta_2}^{R_0} = \frac{\lambda\sigma\eta(\gamma_1+\mu+\mu_1)(1-\alpha)}{\mu(\eta+\mu)(\gamma_1+\mu+\mu_1)(\gamma_2+\mu+\mu_2)} \tag{5.5}$$

$$\chi_{\sigma}^{R_0} = \frac{\lambda\eta\left[\alpha\beta_1(\gamma_2+\mu+\mu_2)+(\gamma_1+\mu+\mu_1)(\beta_2+\tau\mu_2-\alpha\beta_2-\alpha\tau\mu_2)\right]}{\mu(\eta+\mu)(\gamma_1+\mu+\mu_1)(\gamma_2+\mu+\mu_2)} \tag{5.6}$$

$$\chi_{\alpha}^{R_0} = \frac{\lambda\sigma\eta\left[\beta_1(\gamma_2+\mu+\mu_2)-(\gamma_1+\mu+\mu_1)(\beta_2+\tau\mu_2)\right]}{\mu(\eta+\mu)(\gamma_1+\mu+\mu_1)(\gamma_2+\mu+\mu_2)} \tag{5.7}$$

$$\chi_{\tau}^{R_0} = \frac{\lambda\sigma\eta\mu_2(\gamma_1+\mu+\mu_1)(1-\alpha)}{\mu(\eta+\mu)(\gamma_1+\mu+\mu_1)(\gamma_2+\mu+\mu_2)} \tag{5.8}$$

$$\chi_{\eta}^{R_0} = \frac{\lambda\sigma\left[\alpha\beta_1(\gamma_2+\mu+\mu_2)+(\gamma_1+\mu+\mu_1)(\beta_2+\tau\mu_2-\alpha\beta_2-\alpha\tau\mu_2)\right]}{(\eta+\mu)^2(\gamma_1+\mu+\mu_1)(\gamma_2+\mu+\mu_2)} \tag{5.9}$$

$$\chi_{\gamma_1}^{R_0} = -\frac{\lambda\sigma\eta\alpha\beta_1}{\mu(\eta+\mu)(\gamma_1+\mu+\mu_1)^2} \tag{5.10}$$

$$\chi_{\gamma_2}^{R_0} = -\frac{\lambda\sigma\eta\left(\beta_2+\tau\mu_2-\alpha\beta_2-\alpha\tau\mu_2\right)}{\mu(\eta+\mu)(\gamma_2+\mu+\mu_2)^2} \tag{5.11}$$

The table (3) gives the numerical values of the sensitivity:

Sensitivity index	Values
$\chi_{\sigma}^{R_0} = \left(\frac{\partial R_0}{\partial \sigma}\right) \times \left(\frac{\sigma}{R_0}\right)$	1.000000
$\chi_{\beta_1}^{R_0} = \left(\frac{\partial R_0}{\partial \beta_1}\right) \times \left(\frac{\beta_1}{R_0}\right)$	0.350957
$\chi_{\beta_2}^{R_0} = \left(\frac{\partial R_0}{\partial \beta_2}\right) \times \left(\frac{\beta_2}{R_0}\right)$	0.648922
$\chi_{\alpha}^{R_0} = \left(\frac{\partial R_0}{\partial \alpha}\right) \times \left(\frac{\alpha}{R_0}\right)$	−0.081739
$\chi_{\tau}^{R_0} = \left(\frac{\partial R_0}{\partial \tau}\right) \times \left(\frac{\tau}{R_0}\right)$	0.000122
$\chi_{\eta}^{R_0} = \left(\frac{\partial R_0}{\partial \eta}\right) \times \left(\frac{\eta}{R_0}\right)$	0.052133
$\chi_{\gamma_1}^{R_0} = \left(\frac{\partial R_0}{\partial \gamma_1}\right) \times \left(\frac{\gamma_1}{R_0}\right)$	−0.301682
$\chi_{\gamma_2}^{R_0} = \left(\frac{\partial R_0}{\partial \gamma_2}\right) \times \left(\frac{\gamma_2}{R_0}\right)$	−0.573107
$\chi_{\mu_1}^{R_0} = \left(\frac{\partial R_0}{\partial \mu_1}\right) \times \left(\frac{\mu_1}{R_0}\right)$	−0.016090
$\chi_{\mu_2}^{R_0} = \left(\frac{\partial R_0}{\partial \mu_2}\right) \times \left(\frac{\mu_2}{R_0}\right)$	−0.028534

TABLE 3. Sensitivity indices of the model parameters

Figure 4 explicitly shows the effect of each parameter on the endemic threshold. The parameters $\chi_{\beta_1}^{R_0} = 0.350957$, $\chi_{\beta_2}^{R_0} = 0.648922$ and $\chi_{\sigma}^{R_0} = 1.0$ for $R_0 = 1.0597$ are the most positively sensitives. On one hand, the relative infectivity potential of detected infected individuals (β_1), the relative infectivity potential of undetected infected individuals (β_2), and on the other hand, the base transmission rate (σ) has a significant influence on the transmissibility of COVID-19. They contribute to the increase of the endemic threshold and the spread of the epidemic. Furthermore, since β_2 is higher than β_1, this indicates that undetected infected individuals play a greater role in the spread of the epidemic.

The most negatively sensitive parameters are the recovery rate of asymptomatic individuals ($\chi_{\gamma_1}^{R_0} = -0.301682$) and the recovery rate of symptomatic individuals ($\chi_{\gamma_2}^{R_0} = -0.573107$) for $R_0 = 1.0597$. Increasing these recovery rates significantly reduces the number of infectious individuals.

6. Conclusion

In this study, a mathematical model was developed to account for the transmission of COVID-19 through deceased bodies and was applied to Burkina Faso. This model considered susceptible individuals, exposed infected individuals, detected infected individuals, undetected infected individuals, and recovered individuals. The mathematical analysis indicated that the progression of the disease is governed by R_0, the basic reproduction number. Specifically, if $R_0 < 1$, the disease will eventually disappear from the population, leading to a globally and asymptotically stable disease-free equilibrium. Conversely, if $R_0 > 1$, the disease will persist, resulting in a globally and asymptotically stable endemic state.

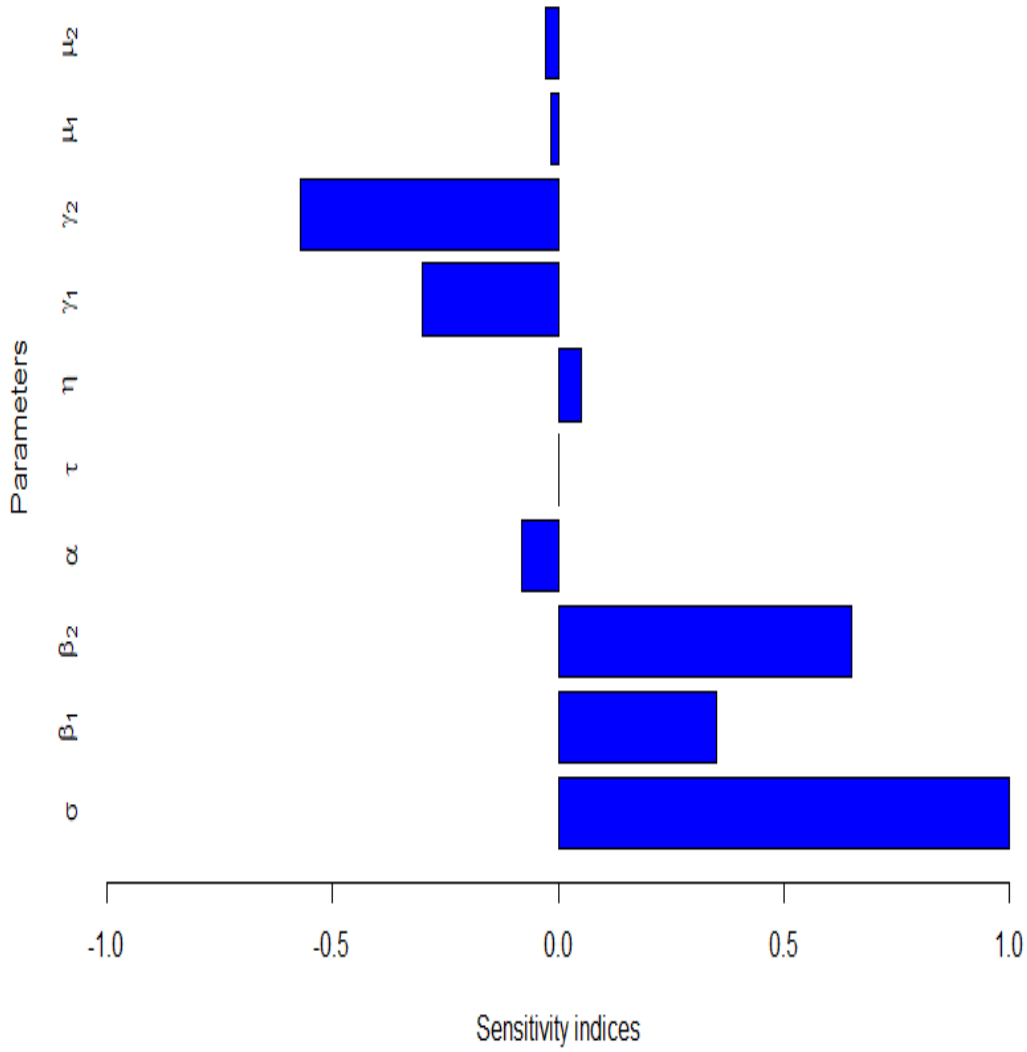

FIGURE 4. sensitivity indices of model parameters

Model parameters were estimated using the AVOA algorithm, based on reported COVID-19 cases in Burkina Faso from March 11 to April 20, 2020. The numerical simulations reveal a slight increase in the number of infected individuals, with a basic reproduction number $R_0 = 1.0597 > 1$, which confirms the low endemicity of COVID-19 in Burkina Faso. Additionally, sensitivity analysis of R_0 highlighted the impact of various parameters on the dynamics of COVID-19 in Burkina Faso, with the most sensitive parameters being the relative potential of detected infected individuals (β_1), the relative potential of undetected infected individuals (β_2), and the transmission rate (σ).

Acknowledgement: The authors wish to express their gratitude to the reviewers for their commitment and the time dedicated to reviewing our article.

Conflicts of Interest: The authors declare that there are no conflicts of interest regarding the publication of this paper.

References

[1] I. Korolev, Identification and Estimation of the SEIRD Epidemic Model for COVID-19, J. Econometrics 220 (2021), 63–85. https://doi.org/10.1016/j.jeconom.2020.07.038.

[2] B.S. Pujari, S. Shekatkar, Multi-City Modeling of Epidemics Using Spatial Networks: Application to 2019-nCov (COVID-19) Coronavirus in India, medRxiv 2020.03.13.20035386, (2020). https://doi.org/10.1101/2020.03.13.20035386.

[3] T. Zhang, Z. Li, Analysis of COVID-19 Epidemic Transmission Trend Based on a Time-Delayed Dynamic Model, Commun. Pure Appl. Anal. 22 (2023), 1–18. https://doi.org/10.3934/cpaa.2021088.

[4] R.K. Singh, M. Drews, M. De La Sen, M. Kumar, S.S. Singh, et al. Short-Term Statistical Forecasts of COVID-19 Infections in India, IEEE Access 8 (2020), 186932–186938. https://doi.org/10.1109/ACCESS.2020.3029614.

[5] R. Niu, E.W.M. Wong, Y.-C. Chan, M.A. Van Wyk, G. Chen, Modeling the COVID-19 Pandemic Using an SEIHR Model With Human Migration, IEEE Access 8 (2020), 195503–195514. https://doi.org/10.1109/ACCESS.2020.3032584.

[6] L. Alyami, S. Das, S. Townley, Bayesian Model Selection for COVID-19 Pandemic State Estimation Using Extended Kalman Filters: Case Study for Saudi Arabia, PLOS Glob. Public Health 4 (2024), e0003467. https://doi.org/10.1371/journal.pgph.0003467.

[7] H.B. Taboe, K.V. Salako, J.M. Tison, C.N. Ngonghala, R. Glèlè Kakaï, Predicting COVID-19 Spread in the Face of Control Measures in West Africa, Math. Biosci. 328 (2020), 108431. https://doi.org/10.1016/j.mbs.2020.108431.

[8] Y. Montcho, R. Nalwanga, P. Azokpota, J.T. Doumatè, B.E. Lokonon, V.K. Salako, M. Wolkewitz, R. Glèlè Kakaï, Assessing the Impact of Vaccination on the Dynamics of COVID-19 in Africa: A Mathematical Modeling Study, Vaccines 11 (2023), 857. https://doi.org/10.3390/vaccines11040857.

[9] A. Guiro, B. Koné, S. Ouaro, Mathematical Modelling of the Evolution Dynamics of the Coronavirus Disease 2019 (COVID-19) in Burkina Faso, in: B. Toni (Ed.), The Mathematics of Patterns, Symmetries, and Beauties in Nature, Springer International Publishing, Cham, 2021: pp. 79–95. https://doi.org/10.1007/978-3-030-84596-4_6.

[10] M. Loibner, C. Langner, P. Regitnig, G. Gorkiewicz, K. Zatloukal, Biosafety Requirements for Autopsies of Patients with COVID-19: Example of a BSL-3 Autopsy Facility Designed for Highly Pathogenic Agents, Pathobiology 88 (2021), 37–45. https://doi.org/10.1159/000513438.

[11] Bereavement Authority of Ontario, COVID-19: Ready...Together, (2022). https://thebao.ca/covid-19-update-links.

[12] British Columbia Centre for Disease Control, Deceased Persons, Provincial Guidance to Ensure the Safety of Workers Handling COVID-19 Suspected or Positive Decedents, (2020). http://www.bccdc.ca/health-professionals/clinical-resources/covid-19-care/deceased-persons.

[13] British Columbia Centre for Disease Control, British Columbia Ministry of Health, Safe Handling of Bodies of Deceased Persons With Suspected or Confirmed COVID-19 (2020). https://medicalstaff.islandhealth.ca/sites/default/files/covid-19/management-and-treatment/covid-safe-handling-suspected-confirmed-deceased-persons-bccdc.pdf

[14] A. Sadollah, H. Sayyaadi, A. Yadav, A dynamic metaheuristic optimization model inspired by biological nervous systems: neural network algorithm, Appl. Soft Comp. 71 (2018), 747–782. https://doi.org/10.1016/j.asoc.2018.07.039.

[15] X. Xiong, S. Li, F. Wu, An enhanced neural network algorithm with quasi-oppositional-based and chaotic sine-cosine learning strategies, Entropy 25 (2023), 1255. https://doi.org/10.3390/e25091255.

[16] H. Fahim, O.W. Sawadogo, N. Alaa, M. Guedda, An efficient identification of red blood cell equilibrium shape using neural networks, Eurasian J. Math. Comp. Appl. 9 (2021), 39–56.

[17] D.E. Goldberg, Real-coded genetic algorithms, virtual alphabets, and blocking, Complex Syst. 5 (1991), 139–167.

[18] A.K. Das, D.K. Pratihar, Solving engineering optimization problems using an improved real-coded genetic algorithm (IRGA) with directional mutation and crossover, Soft Comp. 25 (2021), 5455–5481. https://doi.org/10.1007/s00500-020-05545-9.

[19] R.V. Rao, V.J. Savsani, D.P. Vakharia, Teaching-learning-based optimization: a novel method for constrained mechanical design optimization problems, Computer-Aided Design 43 (2011), 303–315. https://doi.org/10.1016/j.cad.2010.12.015.

[20] S. Mirjalili, S.M. Mirjalili, A. Lewis, Grey wolf optimizer, Adv. Eng. Softw. 69 (2014), 46–61. https://doi.org/10.1016/j.advengsoft.2013.12.007.

[21] Y. Shi, R. Eberhart, A modified particle swarm optimizer, in: IEEE International Conference on Evolutionary Computation Proceedings, IEEE, Anchorage, 1998: pp. 69–73. https://doi.org/10.1109/ICEC.1998.699146.

[22] A. Kiemtore, W.O. Sawadogo, F. Aquel, H. Alaa, K.S. Somda, Mathematical modelling and numerical simulation of hepatitis B viral infection: the case of Burkina Faso, Eur. J. Pure Appl. Math. 17 (2024), 59–92. https://doi.org/10.29020/nybg.ejpam.v17i1.4987.

[23] A. Kiemtore, W.O. Sawadogo, I. Zangré, P.O.F. Ouedraogo, I. Mouaouia, Estimation of parameters for the mathematical model of the spread of hepatitis b in burkina faso using grey wolf optimizer, Int. J. Anal. Appl. 22 (2024), 48. https://doi.org/10.28924/2291-8639-22-2024-48.

[24] F. Aqel, H. Alaa, N.E. Alaa, Mathematical Model of Covid-19 Transmissibility During the Vaccination Period, Eurasian J. Math. Comput. Appl. 11 (2023), 4–28.

[25] I. Tao, T.R. Compaoré, B. Diarra, F. Djigma, T.M. Zohoncon, et al. Seroepidemiology of hepatitis B and C viruses in the general population of burkina faso, Hepat. Res. Treat. 2014 (2014), 781843. https://doi.org/10.1155/2014/781843.

[26] C. Castillo-Chavez, S. Blower, P. Van Den Driessche, D. Kirschner, A.-A. Yakubu, eds., Mathematical approaches for emerging and reemerging infectious diseases: models, methods, and theory, Springer New York, 2002. https://doi.org/10.1007/978-1-4613-0065-6.

[27] O. Koutou, A.B. Diabaté, B. Sangaré, Mathematical analysis of the impact of the media coverage in mitigating the outbreak of COVID-19, Math. Comp. Simul. 205 (2023), 600–618. https://doi.org/10.1016/j.matcom.2022.10.017.

[28] X. Duan, S. Yuan, X. Li, Global stability of an SVIR model with age of vaccination, Appl. Math. Comp. 226 (2014), 528–540. https://doi.org/10.1016/j.amc.2013.10.073.

[29] C. Castillo-Chavez, S. Blower, P. van den Driessche, D. Kirschner, A.A. Yakubu, eds., Mathematical approaches for emerging and reemerging infectious diseases: An introduction, Springer, New York, 2002.

[30] C. Castillo-Chavez, Z. Feng, Global stability of an age-structure model for tb and its applications to optimal vaccination strategies, Math. Biosci. 151 (1998), 135–154. https://doi.org/10.1016/S0025-5564(98)10016-0.

[31] A. Korobeinikov, Lyapunov functions and global stability for SIR and SIRS epidemiological models with non-linear transmission, Bull. Math. Biol. 68 (2006), 615–626. https://doi.org/10.1007/s11538-005-9037-9.

[32] C. Bounkaicha, K. Allali, Y. Tabit, J. Danane, Global dynamic of spatio-temporal fractional order SEIR model, Math. Model. Comp. 10 (2023), 299–310.

[33] R.M. Anderson, R.M. Anderson, R.M. May, Infectious diseases of humans: dynamics and control, Oxford University Press, Oxford, 1991.

[34] National Institute of Statistics and Demography (INSD), General population and housing census, Burkina Faso: Fifth general census of population and housing of Burkina Faso, synthesis of final results, INSD, Ouagadougou, 2019.

[35] J.P. La Salle, The stability of dynamical systems, SIAM, 1976. https://doi.org/10.1137/1.9781611970432.

[36] V. Lakshmikantham, S. Leela, A.A. Martynyuk, Stability analysis of nonlinear systems, Springer, Cham, 2015. https://doi.org/10.1007/978-3-319-27200-9.

[37] A. Khan, R. Zarin, I. Ahmed, A. Yusuf, U.W. Humphries, Numerical and theoretical analysis of rabies model under the harmonic mean type incidence rate, Results Phys. 29 (2021), 104652. https://doi.org/10.1016/j.rinp.2021.104652.

[38] B. Seidu, O.D. Makinde, J.K.K. Asamoah, Threshold quantities and lyapunov functions for ordinary differential equations epidemic models with mass action and standard incidence functions, Chaos Solitons Fractals 170 (2023), 113403. https://doi.org/10.1016/j.chaos.2023.113403.

[39] B. Ivorra, M.R. Ferrández, M. Vela-Pérez, A.M. Ramos, Mathematical modeling of the spread of the coronavirus disease 2019 (COVID-19) taking into account the undetected infections. the case of China, Commun. Nonlinear Sci. Numer. Simul. 88 (2020), 105303. https://doi.org/10.1016/j.cnsns.2020.105303.

[40] R. Li, S. Pei, B. Chen, Y. Song, T. Zhang, W. Yang, J. Shaman, Substantial undocumented infection facilitates the rapid dissemination of novel coronavirus (Sars-Cov-2), Science 368 (2020), 489–493. https://doi.org/10.1126/science.abb3221.

[41] B. Tang, N.L. Bragazzi, Q. Li, S. Tang, Y. Xiao, J. Wu, An updated estimation of the risk of transmission of the novel coronavirus (2019-nCov), Infect. Dis. Model. 5 (2020), 248–255. https://doi.org/10.1016/j.idm.2020.02.001.

[42] N. Ferguson, D. Laydon, G. Nedjati Gilani, N. Imai, K. Ainslie, et al. Report 9: impact of non-pharmaceutical interventions (NPIs) to reduce COVID-19 mortality and healthcare demand, Imperial College London, 2020. https://doi.org/10.25561/77482.

[43] F. Zhou, T. Yu, R. Du, G. Fan, Y. Liu, et al. Clinical course and risk factors for mortality of adult inpatients with COVID-19 in Wuhan, China: A retrospective cohort study, The Lancet 395 (2020), 1054–1062. https://doi.org/10.1016/S0140-6736(20)30566-3.

[44] B. Abdollahzadeh, F. Soleimanian Gharehchopogh, S. Mirjalili, Artificial gorilla troops optimizer: a new nature-inspired metaheuristic algorithm for global optimization problems, Int. J. Intell. Syst. 36 (2021), 5887–5958. https://doi.org/10.1002/int.22535.

[45] Amylia Ait Saadi. Coordination of scout drones (UAVs) in smart-city to serve autonomous vehicles, Thesis, Université Paris-Saclay; Université M'hamed Bougara de Boumerdès, Algérie, 2023.

[46] J.K.K. Asamoah, Z. Jin, G.Q. Sun, Non-seasonal and seasonal relapse model for q fever disease with comprehensive cost-effectiveness analysis, Results Phys. 22 (2021), 103889. https://doi.org/10.1016/j.rinp.2021.103889.

[47] J. Norton, An introduction to sensitivity assessment of simulation models, Environ. Model. Softw. 69 (2015), 166–174. https://doi.org/10.1016/j.envsoft.2015.03.020.